Available online at www.sciencedirect.com
ScienceDirect
International Journal of Heat and Mass Transfer 50 (2007) 4999–5016
International Journal of HEAT and MASS TRANSFER
www.elsevier.com/locate/ijhmt

Flow boiling of liquid nitrogen in micro-tubes: Part I – The onset of nucleate boiling, two-phase flow instability and two-phase flow pressure drop

S.L. Qi [a], P. Zhang [a,*], R.Z. Wang [a], L.X. Xu [b]

[a] Institute of Refrigeration and Cryogenics, Shanghai Jiao Tong University, Shanghai 200240, China
[b] School of Life Sciences and Technology, Shanghai Jiao Tong University, Shanghai 200240, China

Received 29 January 2007; received in revised form 27 June 2007
Available online 23 October 2007

Abstract

This paper is the first portion of a two-part study concerning the flow boiling of liquid nitrogen in the micro-tubes with the diameters of 0.531, 0.834, 1.042 and 1.931 mm. The contents mainly include the onset of nucleate boiling (ONB), two-phase flow instability and two-phase flow pressure drop. At ONB, mass flux drops suddenly while pressure drop increases, and apparent wall temperature hysteresis in the range of 1.0–5.0 K occurs. Modified Thom model can predict the wall superheat and heat flux at ONB. Moreover, stable long-period (50–60 s) and large-amplitude oscillations of mass flux, pressure drop and wall temperatures are observed at ONB for the 1.042 and 1.931 mm micro-tubes. Block phenomenon at ONB is also observed in the cases of high mass flux. The regions for the oscillations, block and stable flow boiling are classified. A physical model of vapor patch coalesced at the outlet is proposed to explain the ONB oscillations and block. Vapor generation caused by the flash evaporation is so large that it should be taken into account to precisely depict the variation of mass quality along the micro-tube. The adiabatic and diabatic two-phase flow pressure drop characteristics in micro-tubes are investigated and compared with four models including homogeneous model and three classical separated flow models. Contrary to the conventional channels, homogeneous model yields better prediction than three separated flow models. It can be explained by the fact that the density ratio of liquid to vapor for nitrogen is comparatively small, and the liquid and vapor phases may mix well in micro-tube at high mass flux due to small viscosity of liquid nitrogen, which leads to a more homogeneous flow. Part II of this study will focus on the heat transfer characteristics and critical heat flux (CHF) of flow boiling of liquid nitrogen in micro-tubes.

Keywords: Micro-tube; Flow boiling; ONB; Pressure drop; Liquid nitrogen

1. Introduction

Flow boiling heat transfer in microchannels is widely applied for many advantages such as high heat flux dissipation and good compactness. One group of the applications mainly includes high heat flux electronic chip cooling, microelectromechanical system (MEMS), etc., where both the operation pressure and mass flow rate are small, and the working fluid is usually water. Another group is the high efficiency and compact air-cooled heat exchangers in both residential and automotive air-conditioning. In this case, the operation pressure and mass flow rate are very large, and the used fluids are various kinds of refrigerants, such as R-134a, R-12, R-141b, R-124, FC-82 and CO_2. For the wide applications, there are many studies on the flow boiling in microchannels.

An important research content for the flow boiling in microchannels is to determine the location of the onset of nucleate boiling (ONB), because the ONB marks the boundary between the single-phase and two-phase heat

* Corresponding author. Tel.: +86 21 34205505; fax: +86 21 34206814.
E-mail address: zhangp@sjtu.edu.cn (P. Zhang).

0017-9310/$ - see front matter © 2007 Elsevier Ltd. All rights reserved.
doi:10.1016/j.ijheatmasstransfer.2007.08.018

Nomenclature

A	cross section area of tube (m^2)
B	Chisholm parameter
c_p	specific heat (J/kg K)
C	constant of L–M model
C_{SF}	shape factor for bubble nucleation
D	hydraulic diameter (m)
e	average surface roughness (μm)
E	Friedel parameter
f	friction factor
F	Friedel parameter
Fr	Friedel number
g	gravitational acceleration (m/s^2)
G	mass flux (kg/m^2 s)
h	heat transfer coefficient (W/m^2 K)
h_{fg}	latent heat of evaporation (J/kg)
H	Friedel parameter
I	electric current through the heater (A)
k	thermal conductivity (W/m K)
L	tube length (mm)
$\dot{m}$	flow rate (kg/s)
Nu	single-phase flow Nusselt number
p	pressure (Pa)
Δp	pressure drop (Pa)
q	average heat flux (W/m^2)
Re	Reynolds number
S	inner surface area of tube (m^2)
T	temperature (K)
ΔT	wall superheat (K)
U	electric voltage across the heater (V)
We	Weber number
x	mass quality
X	Lockhart–Martinelli parameter
z	longitudinal abscissa (m)

Greek symbols

β	contact angle (deg)
ε	void fraction
ϕ	two-phase friction multiplier
Γ	Chisholm parameter
μ	viscosity (kg/m s)
θ	dimensionless temperature
ρ	density (kg/m^3)
σ	surface tension (N/m)
ξ	constant in Thom model

Subscripts

a	acceleration
c	critical point property
crit	critical
eq	equilibrium
exp	experimental
f	friction
flash	flash evaporation
F	fluid
g	gravitation
G	gas
GO	gas only
i	inner surface of tube
in	inlet of tube
L	liquid
LO	liquid only
mea	measured
o	outer surface of tube
out	outlet of tube
pred	predicted
sat	saturation
sc	subcooled
ss	stainless steel
Total	total value
Tp	two-phase
w	wall of tube
z	longitudinal location

transfer regions. Hus [1] was the first to postulate the minimum superheat criterion for the ONB in pool boiling. The criterion declares that the bubble nucleus can grow only if the temperature surrounding the bubble is higher than the saturated temperature corresponding to the pressure inside the bubble. Then Sato and Matasumura [2] and Bergles and Rohsenow [3] extended Hus's criterion to the flow boiling in conventional channels. For the ONB in mini-channels, Hapke et al. [4] studied the ONB in a mini-tube with an internal diameter of 1.5 mm using a thermographic measuring method, and reported that the relatively high wall superheat was necessary to initiate the bubble nucleation. No model could predict the experimental tendency that lower wall superheat is obtained for higher mass flux if the heat flux is kept constant. Hence, they presented a semi-empirical model to predict the heat flux and wall superheat at ONB. Ghiaasiaan and Chedester [5] found that the macroscale models underestimated the heat flux at ONB, and they suggested the thermo-capillary force might suppress the bubble nucleation from the wall cavities. Recently, Liu et al. [6] developed an analytical model to predict the heat flux for ONB of water in the rectangular microchannels which are 275 μm wide by 636 μm deep.

Moreover, complex two-phase flow instabilities, which are undesirable since they can cause problems of system control and lead to thermal fatigue in the heat transfer tubes [7], are usually found in microchannels. Zhang et al. [8] found 4–5 Hz temperature fluctuations with the same frequency to the bubble formation in the flow boiling experiments of deionized water in 113 μm silicon

microchannels. Hetsroni et al. [9] investigated a kind of steady pressure drop fluctuations with low amplitudes and high frequency ranging from 3.6 to 6.6 Hz. They stated the fluctuations were induced by bubble inception and growth behavior. Wu and Cheng [10,11] firstly reported long-period and large-amplitude fluctuations of the temperatures, pressures and mass flux in two sets of parallel microchannels, with hydraulic diameters of 158.8 and 82.8 μm, respectively. They observed the phenomenon that two-phase flow and single-phase flow appear alternatively once the ONB occurs. A recent study by Huh et al. [12] focused on the boiling instability of deionized water in a 103.5 μm single microchannel at very low mass flux and heat flux conditions. They also found the long-period (100–200 s) and large-amplitude fluctuations of the wall temperature, pressure drop and mass flux, and the periodic fluctuations exactly matched the transition of two alternating flow patterns in the micro-tube: a bubbly/slug flow and an elongated slug/semi-annular flow. However, the cause of the oscillations and why this kind of oscillations appear in some cases, but do not in other cases are not clarified.

The two-phase flow pressure drop is also a crucial design parameter for the microchannel systems. Most researchers agree that the two-phase flow pressure drop correlations for the conventional channels are not applicable to the microchannels for the effect of channel diameter on the flow pattern transition [13]. For example, Wen and Kenning [14] found the parameter C in L–M model needed to be modified to predict the data of water during flow boiling in a vertical narrow channel. Similarly, Yu et al. [15] corrected the two-phase multiplier as $\phi_L^2 = X^{-1.9}$ to predict two-phase flow pressure drop of water in a micro-tube with the diameter of 2.98 mm. Lee and Mudawar [16] compared eleven models to their experimental data, and found all the models yielded poor predictions. Zhang and Webb [17] developed a new model based on Friedel correlation for two-phase friction for refrigerants in small-diameter tubes. Revellin and Thome [18] measured two-phase pressure drop over a wide range of experimental conditions in microchannels (single glass tube 0.509 and 0.790 mm in diameter) for R-134a and R-245fa, and proposed a modified homogeneous model.

The fluids in the preceding studies are mainly water and refrigerants, but no research on the flow boiling of liquid nitrogen in microchannels is referred. However, liquid nitrogen owns many applications in micro-cryogenic surgery apparatus (MCSA), the cooling of high temperature superconductivity (HTS) and cryoresistive cables, aerocraft, etc. For example, the inlet tube of the MCSA used to cure various tumors is very small, only about 0.8 mm in diameter; and some channels with the sizes in the range of millimeter or less usually form in the cooling passages of HTS cable-in-conduit conductor (CICC). It is well known that the flow boiling of liquid nitrogen owns distinct features even in traditional channels. Klimenko [19] found the thermophysical properties of the heating surface might affect flow boiling heat transfer of cryogenic fluids. For liquid nitrogen, practically ideal wetting of most solid surfaces and small surface tension may have significant influence on the bubble nucleation, growth and detachment. Moreover, liquid nitrogen also has smaller viscosity, higher thermal conductivity, and smaller density ratio of liquid phase to vapor phase, comparing to the normal fluids (water and refrigerants). These features will undoubtedly affect the heat transfer and pressure drop characteristics of flow boiling in both macro- and microchannels.

Therefore, the flow boiling of liquid nitrogen in the micro-tubes is investigated systemically in the present study. The experiments are preformed in the drawing stainless steel circular tubes with the diameters of 0.531, 0.834, 1.042 and 1.931 mm in the wide range of pressure, mass flux and heat flux. The main contents include the onset of nucleate boiling (ONB), two-phase flow instability, two-phase flow pressure drop, heat transfer characteristics and critical heat flux (CHF). As the first part, this paper introduces the investigation about the ONB, two-phase flow instability, and two-phase flow pressure drop.

2. Experimental apparatus and procedures

2.1. The test loop

The schematic illustration of the test loop is presented in Fig. 1. Liquid nitrogen in the storage tank is supplied to the experimental micro-tube section by gaseous nitrogen from a high-pressure nitrogen gas cylinder. One reductor and a pressure control valve connected to the nitrogen gas cylinder are used to control the system pressure. To reduce the heat leakage from the ambient, both the storage tank and test section are installed in a vacuum dewar. Two rows of filter are placed upstream the micro-tube to avoid the frazil and other impurities blocking in the flow passage. A flow rate control valve located at the outlet of the test section is used to control the flow rate. After passing the valve, liquid nitrogen go through an evaporator immersed in a 20 °C water bath and evaporates completely. Finally, the mass flux of nitrogen gas is measured by an Alicat® mass flow meter with a calibration accuracy of ±0.8%.

2.2. The test section

Fig. 2 illustrates the configuration of the test section, which is a modified version of previous experimental setup [20]. The test section is installed vertically in the vacuum dewar, and liquid nitrogen flows upward through the micro-tube. The micro-tube and the inlet/outlet flanges are soldered together. To ensure the flow stability, there is a mixing chamber at the inlet and outlet of the test section, respectively. The chamber and test section flange are bonded together with six bolts. The test section is divided into three subsections. Section 1 is heated only while the two-phase frictional pressure drop multiplier is investigated. At that time, heat flux is input from Section I, and Section II is kept adiabatic. By adjusting the input heat

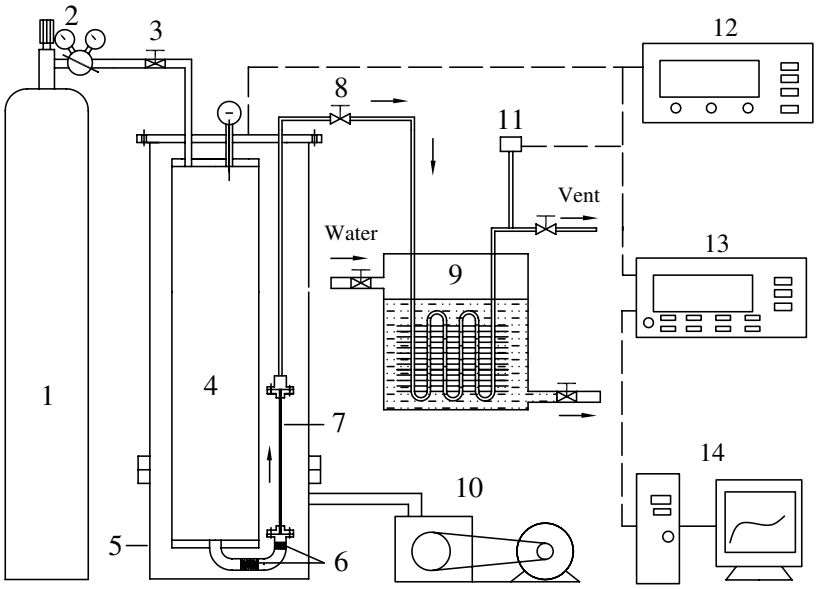

1. Nitrogen gas cylinder
2. Reductor
3. Pressure control valve
4. Liquid nitrogen storage tank
5. Vacuum dewar
6. Filter
7. Test section
8. Flow rate control valve
9. Evaporator
10. Vacuum pump
11. Mass flow meter
12. DC power controller
13. Data acquisition device
14. Computer

Fig. 1. The schematic illustration of the experimental apparatus.

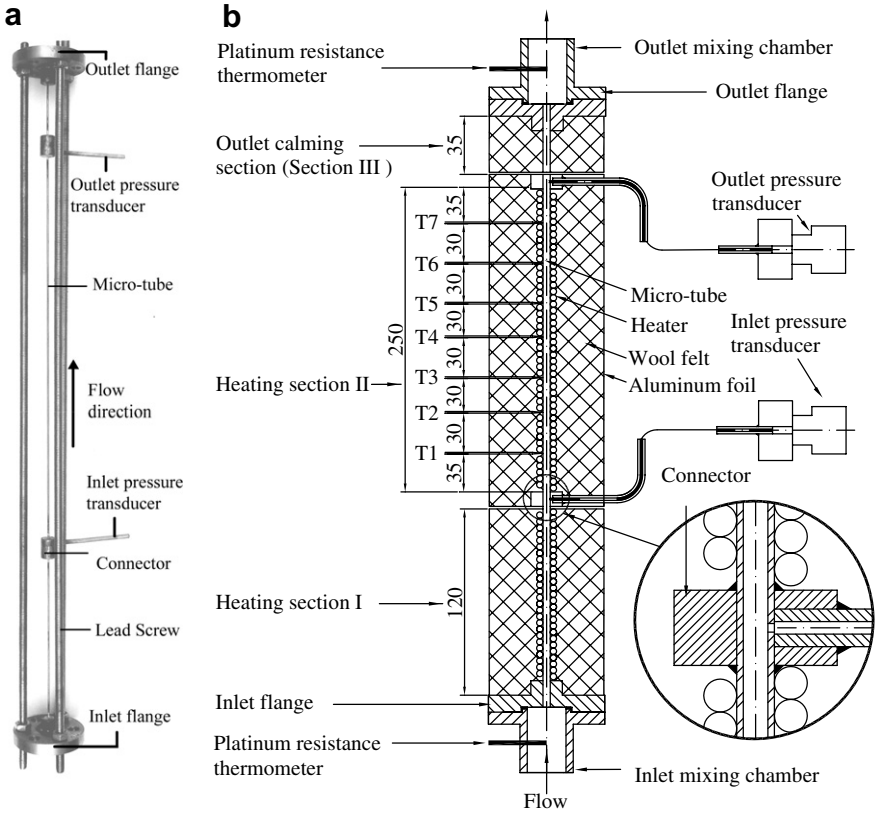

Fig. 2. The photograph and schematic illustration of the test section: (a) photograph; (b) schematic illustration.

flux, two-phase flow with different inlet mass quality for Section II can be obtained. While two-phase flow goes through the adiabatic Section II, two pressure taps at two ends can measure the pressure drop. These pressure taps are directly set through the micro-tube wall, and then are connected to the absolute pressure transducers, as shown in Fig. 2. While studying the flow boiling heat transfer and related diabatic two-phase flow, Section II is heated, and Section I is kept adiabatic. Section III is the outlet calming section, which is connected downstream Section II and always kept adiabatic. The vessel pressure is also simultaneously measured by another pressure transducer. The uncertainty of the pressure measurement is within ±0.3 kPa by a standard calibration.

Fluid temperatures at the inlet and outlet of the experimental section are measured by using the platinum resistance thermometers with an accuracy of about ±0.1 K. Seven T-type (copper-constantan) thermocouples with a diameter of 0.1 mm are soldered on the outer surface of the micro-tube to measure the wall temperature. Prior to the installation, all the thermocouples are calibrated by a Lakeshore® temperature sensor with an accuracy of about ±0.1 K.

The test channels are the commercial stainless steel (ss, Type 304) tubes, which are usually used to fabricate the medical injectors. The tube diameters are precisely measured by using a 500× microscope, whose measurement accuracy is ±0.001 mm. Meanwhile, the average roughness of the micro-tubes is also measured by Acuor Alpha-step 500® surface profiler. Overall, four tubes are tested, and their dimensions and the measured average roughness are given in Ref. [20].

The heater is the manganin wire with a diameter of 0.18 mm, which is tightly coiled around the micro-tube. It should be noted that the wire must be coiled carefully to avoid contacting with the thermocouples. Then a thin layer of cryogenic glue is uniformly painted around the micro-tube to ensure the uniformity of the input heat flux. The heat flux is adjusted by changing the electric current delivered from the DC power (the maximum power is 360 W). Wool felt and aluminum foil are orderly wrapped around the heater to reduce the heat leakage. Overall heat loss including the heat radiation to the ambient and heat conduction from the ends of the micro-tube is estimated to be less than 5% of the input power. The result is verified by heat balance between the ohmic heat input and the sensible heat increase of the fluid for single-phase flow.

2.3. The test procedures

Before each experiment run, the dewar containing the test section is precooled to about 150 K, and evacuated by a mechanical vacuum pump to 2.0–5.0 Pa. All the data are collected when the experiment reaches a steady state defined in such a way that the pressure drop and the wall temperature fluctuate within ±5% and ±0.1 K, respectively. Then the outputs of the thermocouples, electric current and voltage, flow meter and pressure transducers are recorded by a data logger (Keithley® 2700) and stored in a computer for further analysis. The experiments are carried out within wide range of operating conditions, as listed in Table 1, which includes the ranges of the inlet temperature, T_{in}, inlet pressure, p_{in}, outlet pressure, p_{out}, mass flux, G, and heat flux, q.

Table 1
Operating conditions of the experiments

No.	D_i (mm)	T_{in} (K)	p_{in} (kPa)	p_{out} (kPa)	G (kg/m^2 s)	q (W/cm^2)
1	0.531	78.2–79.8	370–920	180–450	700–3000	5.17–15.28
2	0.834	78.2–79.8	300–890	200–580	820–2630	5.09–21.39
3	1.042	78.2–79.8	270–580	160–520	590–1420	6.44–14.85
4	1.931	78.2–79.8	180–240	140–190	440–920	6.38–14.62

3. Data reduction and uncertainty analysis

3.1. Heat flux and wall temperature

The heat flux is determined by the input electric voltage and current through the heater

$$q = \frac{UI}{S} \tag{1}$$

The inner wall temperature is determined with a correction to the temperature drop over the wall thickness

$$T_{w,i} = T_{w,o} - \frac{qD_i \ln(D_o/D_i)}{2k_{ss}} \tag{2}$$

3.2. Length of the subcooled section

For the small latent heat of evaporation, liquid nitrogen is usually kept subcooled to avoid the vaporization before entering the inlet of test section. Hence, there is one section called subcooled section, whose length must be determined for the calculation of the two-phase pressure drop and the saturated temperature along the micro-tube. The length of the subcooled section is obtained from the iteration of the following equations including the heat balance Eq. (3), the saturated vapor pressure Eq. (4) and the single-phase pressure drop Eq. (5)

$$L_{sc} = \frac{GAc_{p,L}(T_{sat,sc} - T_{in})}{\pi Dq} \tag{3}$$

$$T_{sat,sc} = func(p_{sat,sc}) \tag{4}$$

$$p_{sat,sc} = p_{in} - f\frac{G^2}{2\rho_L}\frac{L_{sc}}{D} \tag{5}$$

where the saturated vapor pressure equation is

$$\ln\left(\frac{p_{sat}}{p_c}\right) = \left(\frac{T_c}{T_{sat}}\right)\left[N_1\theta + N_2\theta^{1.5} + N_3\theta^{2.5} + N_4\theta^5\right] \tag{6}$$

and where $\theta = 1 - T_{sat}/T_c$, $N_1 = -6.1245$, $N_2 = 1.2633$, $N_3 = -0.7659$, $N_4 = -1.7757$.

According to the pressure drop results for single-phase flow of liquid nitrogen [20], the friction factor, f, can be determined by Colebrook correlation

$$\frac{1}{\sqrt{f}} = -2.0\log\left(\frac{e/D}{3.7} + \frac{2.51}{Re\sqrt{f}}\right) \tag{7}$$

where the relative surface roughness e/D is given in Ref. [20].

3.3. Mass quality along the micro-tube

Along the micro-tube, local mass quality is

$$x(z) = x_{\mathrm{eq}}(z) + x_{\mathrm{flash}}(z) \tag{8}$$

where equilibrium mass quality, $x_{\mathrm{eq}}(z)$, is calculated as

$$x_{\mathrm{eq}}(z) = \frac{\pi D(z - L_{\mathrm{sc}})q}{AGh_{\mathrm{fg}}} \tag{9}$$

And x_{flash} is the mass quality generated by flashing of the liquid during the two-phase flow. For the two-phase flow in micro-tube, the pressure gradient is considerably large, which results in the decrease of the saturation temperature corresponding to the local pressure. While the liquid temperature is higher than the saturation temperature, flashing of liquid occurs. x_{flash} can be obtained by

$$x_{\mathrm{flash}}(z) = \frac{c_{p,\mathrm{L}}(T_{\mathrm{sat}}(L_{\mathrm{sc}}) - T_{\mathrm{sat}}(z))}{h_{\mathrm{fg}}} \tag{10}$$

3.4. Two-phase pressure drop

The two-phase pressure drop gradient along the micro-tube consists of three components, i.e., acceleration, friction and gravitation pressure drop gradients:

$$\frac{\mathrm{d}p}{\mathrm{d}z} = \frac{\mathrm{d}p_{\mathrm{a}}}{\mathrm{d}z} + \frac{\mathrm{d}p_{\mathrm{f}}}{\mathrm{d}z} + \frac{\mathrm{d}p_{g}}{\mathrm{d}z} \tag{11}$$

where the acceleration and gravitation pressure drop gradient components are respectively written as

$$\frac{\mathrm{d}p_{\mathrm{a}}}{\mathrm{d}z} = \frac{\mathrm{d}}{\mathrm{d}z}\left\{G^2\left[\frac{(1-x)^2}{\rho_{\mathrm{L}}(1-\varepsilon)} + \frac{x^2}{\rho_{\mathrm{G}}\varepsilon}\right]\right\} \tag{12}$$

$$\frac{\mathrm{d}p_{g}}{\mathrm{d}z} = [\rho_{\mathrm{G}}\varepsilon + \rho_{\mathrm{L}}(1-\varepsilon)]g \tag{13}$$

The void friction, ε, and the friction pressure drop gradient component, $\mathrm{d}p_{\mathrm{f}}/\mathrm{d}z$, vary with different models including the homogeneous model, and three separated flow models adopted in the present study, i.e., Lockhart–Martinelli (L–M) model, Chisholm B coefficient model and Friedel model.

After the determination of the above three pressure drop gradient components, the pressure drop at z can be obtained by the integral. For example, the pressure drop component Δp_{a} is calculated by

$$\Delta p_{\mathrm{a}}(z) = \int_0^z \frac{\mathrm{d}p_{\mathrm{a}}}{\mathrm{d}z}\mathrm{d}z \tag{14}$$

The total pressure drop of the two-phase flow, $\Delta p_{\mathrm{Total}}$, is the sum of three components

$$\Delta p_{\mathrm{Total}} = \Delta p_{\mathrm{a}} + \Delta p_{g} + \Delta p_{\mathrm{f}} \tag{15}$$

3.5. Two-phase frictional pressure drop multipliers

Two-phase frictional pressure drop multipliers is defined as

$$\phi_{\mathrm{LO}}^2 = \frac{\Delta p_{\mathrm{Tp}}}{\Delta p_{\mathrm{LO}}} \tag{16}$$

where Δp_{Tp} is obtained by subtracting the gravitational pressure drop from the measured pressure drop

$$\Delta p_{\mathrm{Tp}} = p_{\mathrm{in}} - p_{\mathrm{out}} - [(1-\varepsilon)\rho_{\mathrm{L}} + \varepsilon\rho_{\mathrm{G}}]gL \tag{17}$$

where the void fraction ε is calculated according to the homogeneous model

$$\varepsilon = \frac{\rho_{\mathrm{L}}/\rho_{\mathrm{G}}}{1/x_{\mathrm{out}} + (\rho_{\mathrm{L}}/\rho_{\mathrm{G}} - 1)} \tag{18}$$

and x_{out} is the quality at the outlet of the heating Section I, and is deduced by the method in Section 3.3. Moreover, the single-phase pressure drop Δp_{LO} is

$$\Delta p_{\mathrm{LO}} = f\frac{L}{D}\frac{G^2}{2\rho_{\mathrm{L}}} \tag{19}$$

where the friction factor, f, is given by Eq. (7).

3.6. Uncertainty analysis

Based on the measurement uncertainties of the tube diameter, tube length, temperature, pressure difference and mass flow rate, the uncertainties of the derived parameters including the heat flux, mass flux, Reynolds number and mass quality can be calculated using propagation analysis [21]. Main experimental uncertainties are summarized in Table 2. It can be seen that the uncertainties of Re and x are no more than ±2.0% and ±3.2%, respectively.

Table 2
Summary of the uncertainty analysis

Parameter	Uncertainty
Parameter measurement	
Diameter, D (mm)	±0.001
Length, L (mm)	±1.0
Temperature, T (K)	±0.1
Pressure difference, P (kPa)	±0.3
Mass flow rate, $\dot{m}$ (%)	±0.8
Parameter derived	
Heat flux, q (%)	±5.0
Mass flux, G (%)	±0.9
Reynolds number, Re (%)	±2.0
Mass quality, x (%)	±3.2

4. Results and discussion

4.1. Onset of nucleate boiling (ONB)

4.1.1. ONB and the flow boiling curve

Fig. 3 shows one example of the variations of mass flux, pressure drop, and wall temperature at the onset of nucleate boiling (ONB). Different from the conventional channels, ONB for the micro-tube displays distinct features for mass flux, pressure drop and wall temperature. In details, the mass flux decreases abruptly while the pressure drop increases at ONB, and there is a sudden drop of wall temperature with the amplitude of 1.0–5.0 K, which is called the temperature hysteresis. At ONB, a bubble will nucleate, grow and depart from the active nucleate cavity at the heating wall, and the vaporization causes apparent volume expansion, which makes the mass flux drop rapidly. It is well known that the pressure drop of two-phase flow is much larger than that for the single-phase flow, even decade times in some cases. As a consequence, the pressure drop increases from 148.5 to 259.5 kPa though the mass flux decreases from 3271.4 to 1961.5 kg/m^2 s. The temperature hysteresis results from the transition of heat transfer mechanism from the single-phase forced convection to the two-phase flow boiling. With the same heat flux, the heat transfer coefficient of the flow boiling is higher than that of the forced convection; hence the temperature difference and the wall temperature drop. From Fig. 3(d), it can be seen that ONB occurs at the outlet first, and moves upstream gradually with the increase of heat flux. Meanwhile, the wall temperature at ONB gradually increases when the ONB moves upstream.

From the flow boiling curve depicted in Fig. 4, two heat transfer regions, i.e., the single-phase forced convection region and the flow boiling region, can be clarified clearly by the ONB. In the single-phase forced convection region, the temperature difference increases almost linearly with the heat flux. While in the two-phase flow boiling region, the temperature difference at T5 increase slowly,

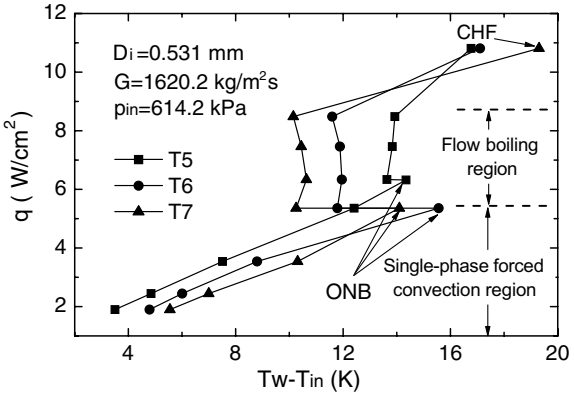

Fig. 4. Flow boiling curve for 0.531 mm micro-tube.

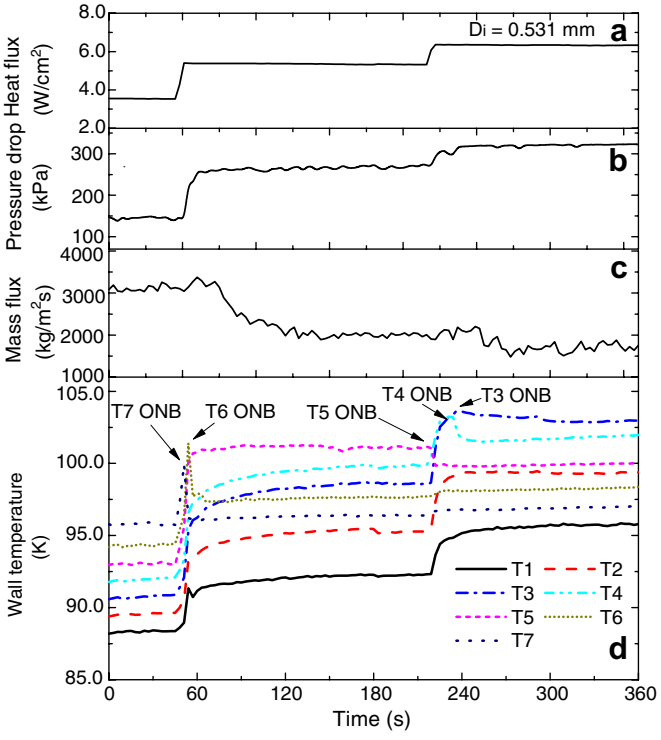

Fig. 3. Variation of the parameters at the onset of nucleate boiling (ONB) for 0.531 mm micro-tube: (a) heat flux; (b) pressure drop; (c) mass flux; (d) wall temperature.

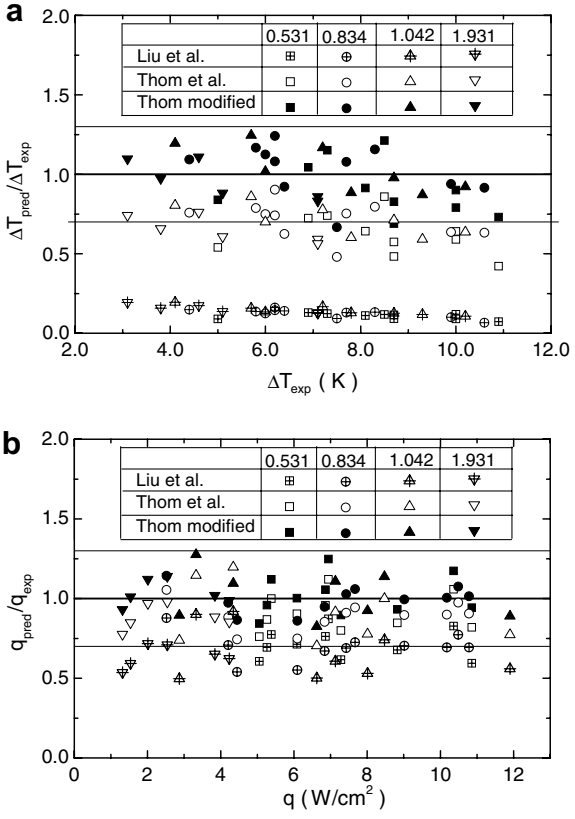

Fig. 5. Comparison of the wall superheat and heat flux at ONB between the experimental data and the predicted results: (a) the wall superheat; (b) heat flux.

even decreases at T6 and T7 for the drop of the saturated temperature corresponding to the decreased saturated pressure. Moreover, the critical heat flux (CHF) is also marked at 11.04 W/cm^2.

4.1.2. ONB analytical model and experimental data

Up to now, there are many models to predict the wall superheat and heat flux triggering the ONB. For example, the model proposed by Thom [22] is

$$T_w - T_{sat} = \xi\left(\frac{q}{1.0\times 10^6}\right)^{0.5}\exp\left(-\frac{p}{8.7\times 10^6}\right) \tag{20}$$

with the constant $\xi = 22.65$. Recently, Liu et al. [6] developed one superheat criterion for the prediction of ONB

$$\sqrt{T_w} - \sqrt{T_{sat}} = \sqrt{\frac{2\sigma C_{SF}}{\rho_G h_{fg}}\frac{q}{k_F}} \tag{21}$$

where C_{SF} is the shape factor, $C_{SF} = 1 + \cos\beta$.

In most cases, however, with the given inlet pressure, inlet temperature, micro-tube length and mass flux, the wall temperature and heat flux at ONB need to be determined. As a consequence, an iterating process is required. The wall temperature can be calculated by heat transfer equation

$$T_{w,z} = T_{F,z} + \frac{q}{Nuk_F/D} \tag{22}$$

where $T_{F,z}$ can be obtained by

$$T_{F,z} = T_{F,in} + \int_0^z \frac{qS}{GAc_{p,L}(z)L}\mathrm{d}x \tag{23}$$

The saturated temperature T_{sat}, in Eqs. (20) and (21), is determined according to the saturated pressure, $p_{sat,z}$, through Eq. (6), and $p_{sat,z}$ is obtained by

$$p_{sat,z} = p_{in} - f\frac{G^2}{2\rho_L}\frac{z}{D} \tag{24}$$

Table 3
Experimental data and predicted results by the modified Thom model for the wall temperature and heat flux at ONB

D_i (mm)	Case	G (kg/m^2 s)	T_{in} (K)	p_{in} (kPa)	$T7_{exp}$ (K)	q_{exp} (W/m^2)	$T7_{pred}$ (K)	q_{pred} (W/m^2)
0.531	1	3044.7	79.2	469.102	99.9	53830.9	98.4	60330.1
	2	2500.2	78.8	473.249	100.9	52584.1	98.5	50439.4
	3	2326.7	79.3	426.766	99.5	50519.1	96.8	42584.6
	4	3160.1	79.3	744.465	107.6	88243.9	106.0	82288.4
	5	3006.4	78.3	617.997	105.1	68598.8	103.0	72454.2
	6	4173.2	78.6	842.590	107.2	103605.9	109.0	121553.2
	7	2845.8	79.2	555.631	100.7	60813.7	101.1	60984.8
	8	3554.1	79.1	663.304	102.9	69416.8	104.1	86651.9
	9	3186.4	78.4	496.863	100.0	72816.6	99.3	65251.6
	10	4741.2	79.1	582.584	102.0	108561.7	101.2	102353.4
0.834	1	2091.4	78.6	273.342	92.2	44467.7	91.7	38484.2
	2	2306.1	79.3	350.033	95.0	60930.7	95.5	52460.9
	3	2540.3	79.9	504.616	99.5	74291.2	101.2	76355.5
	4	2474.3	78.6	620.871	104.0	90160.3	105.3	89649.6
	5	2091.4	78.5	493.528	99.9	68351.7	101.1	64831.8
	6	2208.8	78.7	613.171	105.6	101744.5	105.4	102314.8
	7	1111.4	78.5	427.373	99.4	25177.1	96.9	28791.2
	8	2690.7	78.6	780.302	109.9	104876.9	109	112742.1
	9	1544.5	78.7	423.897	97.1	42016.6	97.6	40926.3
	10	2529.3	78.9	518.947	101.4	76676.9	102.2	81260.2
	11	2953.5	79.3	651.296	104.7	107807.8	106.4	109375.3
1.042	1	1476.0	78.8	384.569	96.6	33289.5	96.7	42453.1
	2	1886.4	78.8	404.375	96.8	53410.3	98.2	58513.0
	3	1762.5	78.8	206.364	87.2	28728.2	88.0	25705.2
	4	2877.3	78.9	311.544	96.5	80103.8	95.3	74097.8
	5	2271.9	78.5	288.053	94.5	66239.9	93.6	54600.4
	6	2986.7	79.6	474.712	102.8	119019.5	102.1	105930.2
	7	2665.9	79.7	503.416	102.2	84746.9	102.3	96469.4
	8	3190.1	78.0	277.788	92.7	71324.7	93.9	79083.0
1.931	1	897.2	79.2	192.279	86.8	15342.9	86.7	15495.9
	2	816.9	79.3	181.749	85.5	13170.3	85.8	12254.2
	3	1126.2	79.2	244.642	90.1	25427.9	90.6	28965.7
	4	1346.2	78.3	260.831	93.3	42345.8	92.3	41835.3
	5	950.4	78.5	220.364	89.5	20110.5	88.9	22539.6
	6	1276.5	78.1	255.867	93.1	38416.7	91.9	39196.3

Substituting T_w and T_{sat} into the criterion of Eq. (20) or (21), the heat flux at the ONB can be obtained by the iteration. Meanwhile, the wall temperature and wall superheat $\Delta T = T_w - T_{sat}$ at the ONB are also calculated.

In Fig. 5, the measured wall superheat and heat flux at ONB for various inlet pressure, inlet fluid temperature and mass flux are compared with the predictions by Thom model and Liu model. It can be seen that both models obviously underestimate the experimental data. Especially for the Liu model, $\Delta T_{pred}/\Delta T_{exp}$ is less than 0.25 for all the data. For the heat flux, two models also show a systematic underestimation. There may be two reasons for this large derivation. Firstly, the two models are based on the criterion for the pool boiling, and do not take the influence of space into account. However, the wall superheat criterion may have been changed for the micro-tube. Peng and Wang [23] found that a relative high wall superheat is necessary for the ONB in the microchannel. Secondly, the large mass flux may suppress the bubble nucleation in the microchannels [24,25]. Hence, the wall superheat criterion for the ONB must be increased to fit the experimental data. From Figs. 5(a) and (b), one can find that $\Delta T_{pred}/\Delta T_{exp}$ and q_{pred}/q_{exp} for Thom model almost keep constant with the variation of ΔT and q, which means Thom model can correctly predict the tendencies of ΔT and q though it does not work well quantitatively. It seems that the constant ξ in Thom model is not applicable for the present micro-tubes. Analysis shows that a better fitting to the experimental data can be obtained by modifying ξ from 22.65 to 30.65, as shown in Fig. 5. In detail, the measured wall temperature and heat flux at ONB and the predictions by the present fitting are listed in Table 3.

4.2. Two-phase flow instability

4.2.1. Oscillations at ONB

At $p_{in} = 551.875$ kPa, $G = 3136.5$ kg/m^2 s, and $q = 8.27$ W/cm^2, a kind of oscillation phenomenon is observed at ONB for the micro-tube with a diameter of 1.042 mm, as shown in Fig. 6 (for the cases of oscillations at ONB, the values of parameters p_{in} and G are these at the point of ONB). If the system pressure, heat flux and outlet conditions do not change significantly, the oscillation enables to be sustained continuously. Hence, it is a kind of stable oscillation. Moreover, it is also a kind of long-period and large-amplitude oscillation for the oscillation period is about 60 s, and the oscillation amplitudes for the pressure drop and mass flux are about 30 kPa and 2250 kg/m^2 s, respectively, as shown in Fig. 6(a). The phase difference between the pressure drop and mass flux oscillations is about 180°, i.e., the wave crest of mass flux corresponds to the wave hollow of pressure drop, and the wave hollow

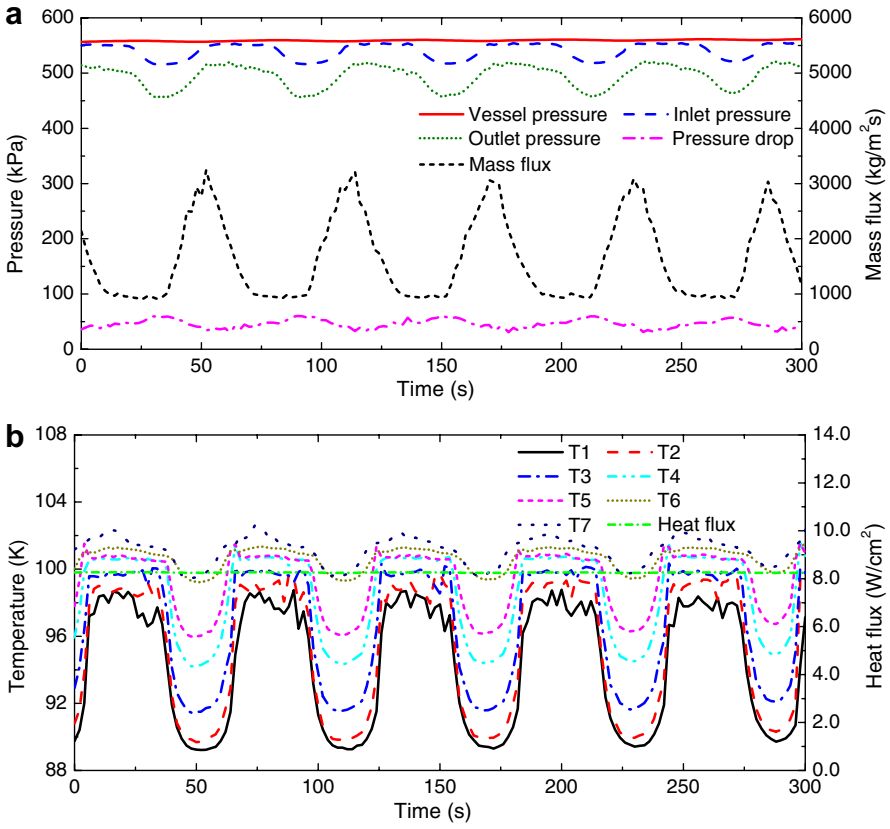

Fig. 6. Boiling onset oscillations for 1.042 mm micro-tube ($p_{in} = 551.875$ kPa, $G = 3136.5$ kg/m^2 s, $q = 8.27$ W/cm^2): (a) pressure and mass flux; (b) wall temperature and heat flux.

of mass flux corresponds to the wave crest of pressure drop. Meanwhile, the wall temperatures from T1 to T7 also fluctuate corresponding to the mass flux and pressure drop, as shown in Fig. 6(b). The oscillation amplitudes of wall temperature are in the range of 2.9–9.4 K, and the oscillations own the phase opposite to the mass flux, but same to the pressure drop.

By the assistant of the schematic illustration of the outlet configuration of the experimental setup shown in Fig. 7, the oscillation process can be explained qualitatively as follows: after the ONB, many small bubbles flow out the micro-tube, ant enter the mixing chamber (also called the plenum). Since the mixing chamber is a conventional channel with much larger diameter than the micro-tube, the velocity of the bubbles may decrease. Hence the inertia force turns weak, whereas the effect of gravitational force turns significant, and the bubbles usually accumulate at the upper part of due to the small density of vapor. As shown in Fig. 7(a), one vapor patch is formed at the entrance of the outlet valve (or constraint). Hence, the mass flux drops gradually, which causes the increase of the wall temperature and the two-phase flow quality in the micro-tube. Correspondingly, higher quality leads to larger pressure drop. When the vapor patch is discharged, liquid phase will fill in the outlet mixing chamber and the micro-tube, as shown in Fig. 7(b). The mass flux begins to increase, which causes better heat transfer and the decrease of the wall temperatures. The pressure drop also decreases for the friction factor of the single-phase flow is much smaller than that of the two-phase flow, though there is a growth of the mass flux. With the constant heat flux, the ONB will occur again, and the oscillations repeat.

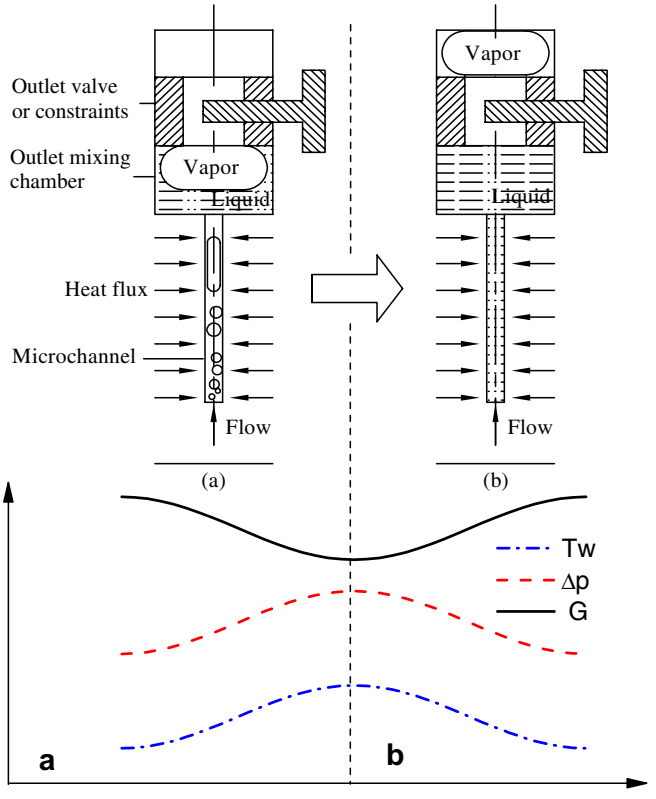

Fig. 7. The schematic illustration of the physical model of the oscillations at ONB.

Essentially, the oscillations observed in the present study are caused by the vapor patch coalesced at the entrance of the outlet valve. The existence of the vapor patch causes the transition of flow patterns through the valve, i.e., liquid phase and vapor phase occur alternately. The transition of flow patterns at the outlet (macro-channel) affects the flow and heat transfer in the micro-tube, and leads to the present oscillations. This can explain why the oscillation period is so long. The present oscillations are quite different from those observed by Zhang et al. [8] and Hetsroni et al. [9], which are short-period oscillations caused by the bubble inception and detachment in microchannels. Moreover, the outlet pressure is very high (about 520 kPa in Fig. 6(a)) at ONB oscillation, which indicates the blockage at the outlet is very strong. As shown in Fig. 6(b), the oscillation amplitude of the wall temperature decreases along the flow direction, from 9.4 K for T1 to 2.9 K for T7. This is because the flow pattern transition between single-phase and two-phase is most impetuous at T1.

For 1.042 mm micro-tube, Table 4 presents the oscillation periods and amplitudes with different inlet pressure and mass flux. Generally speaking, the periods of the oscillation are in the range of 50–60 s. It can be seen that higher inlet pressure and mass flux correspond to shorter period and larger amplitude of the wall temperature. The tendency of period with mass flux can be interpreted by the physical model of vapor patch coalesced at the outlet. The time required for coalescing the vapor patch decreases, and the period turns short with the increase of mass flux.

For 1.931 mm micro-tube, the similar oscillations are also observed. Fig. 8 is an example at $p_{in} = 280.505$ kPa, $G = 1236.5$ kg/m^2 s, and $q = 3.31$ W/cm^2. It can be seen that the oscillation period is about 54 s. Compared with the oscillation for 1.042 mm micro-tube, the amplitude of wall temperature is very large. For example, the amplitude of T7 even reaches 74.6 K, which suggests that the local dryout occurs at this place.

4.2.2. Block at ONB

The region of the ONB oscillations is very narrow, and a kind of block at ONB is usually observed for the high inlet pressure and mass flux in the present experiments. Fig. 9(a) shows the variations of pressure and mass flux before and

Table 4
The oscillations at ONB for 1.042 mm micro-tube

No.	p_{in} (kPa)	G (kg/m^2 s)	q (W/m^2)	Amplitude of the wall temperature (K)	Period (s)
1	467.556	2923.7	79948.5	2.5–7.8	65
2	551.875	3136.5	82738.4	2.9–9.4	60
3	521.496	3424.4	89243.2	2.6–9.7	54
4	584.949	3287.2	88327.9	3.8–9.9	53
5	691.637	3401.3	87453.9	4.8–10.2	50

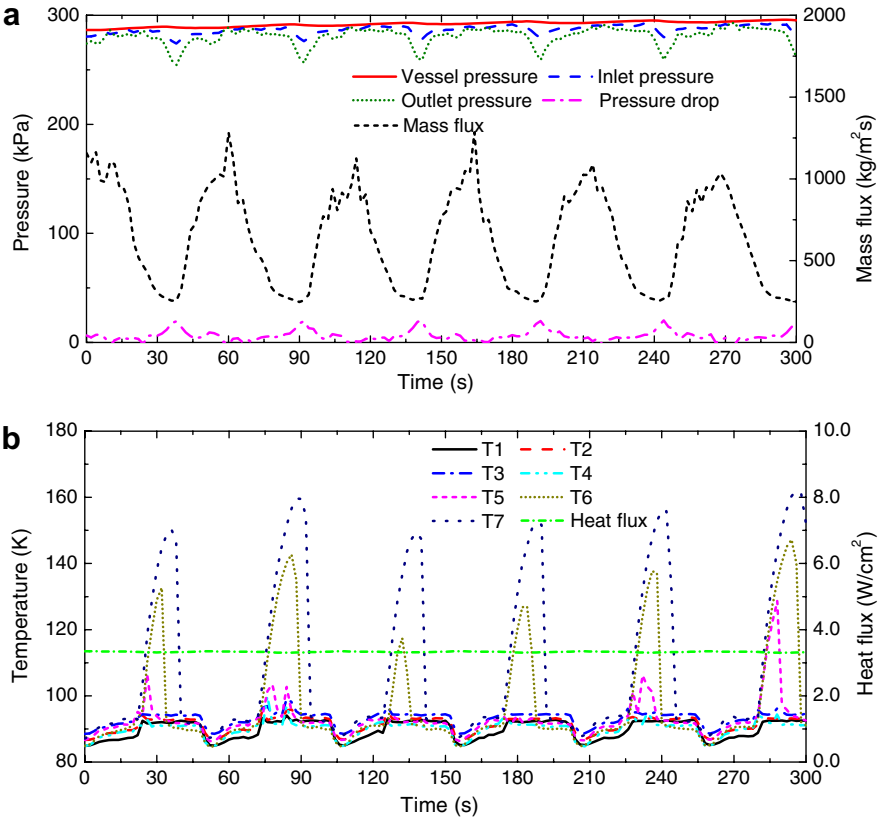

Fig. 8. Boiling onset oscillations for 1.931 mm micro-tube ($p_{in} = 280.505$ kPa, $G = 1236.5$ kg/m^2 s, $q = 3.31$ W/cm^2): (a) pressure and mass flux; (b) wall temperature and heat flux.

after the ONB block, and Fig. 9(b) presents the variations of heat flux and wall temperature. At first, the flow in the micro-tube is single-phase convection in the range of low heat flux. The pressure drop decreases gradually, while the mass flux basically keeps constant with the step increase of heat flux. This is because the viscosity of liquid nitrogen decreases due to the input of heat flux [20]. All the wall temperatures from T1 to T7 increase with the heat flux. The block occurs at about 500 s where $p_{in} = 606.439$ kPa, $T_{in} = 79.3$ K, $G = 2186.1$ kg/m^2 s, and $q = 7.70$ W/cm^2. The mass flux drops rapidly, whereas the pressure drop increases abruptly, and the wall temperatures at T6 and T7 soar to 140 and 170 K, respectively.

According to the method mentioned in Section 3.2, the length of subcooled section L_{sc} is determined to be 248 mm, nearly equal to the total heating length of 250 mm, which indicates that the micro-tube is blocked once the ONB occurs near the outlet. The reason for the block can also be explained according to the model illustrated in Fig. 7. After a vapor patch is coalesced at the entrance of the outlet valve, the block occurs if the discharge rate of the vapor patch is less than the flow rate through the micro-tube. Then the dryout will appear in the micro-tube because the produced vapor cannot be discharged, which causes abrupt increase of the wall temperature. In fact, the block disappears if the constraint caused the outlet valve is removed.

This kind of ONB block has some similar features to the critical heat flux (CHF), but the triggering conditions and mechanism are different. For 1.042 mm micro-tube, the parameters for the ONB block and CHF are listed in Table 5. It can be seen that the heat flux and the outlet quality x_{out} for the ONB block are much smaller than those for the CHF. While the ONB blocks are observed, the ONB always occurs at the end of the micro-tube. Though both the ONB block and CHF own the dryout phenomenon, the mechanisms leading to the dryout are not the same. For the ONB block, the flow is stopped, and no liquid can enter the micro-tube to wet the wall surface. Hence, the wall temperature soars. However, dryout of the liquid film near the outlet is widely regarded as the trigger mechanism for the CHF.

4.2.3. Classification of stable and unstable regions

The ONB oscillation of mass flux, pressure drop and wall temperature is a kind of two-phase dynamic instability. It is undesirable because it may cause problems of system control and premature thermal fatigue in the tube [26]. Similarly, the designers also make efforts to avoid the ONB block, which may induce a large accidental increase in surface temperature and catastrophic system failure. Thus, it is imperative to classify the stable region and unstable region. Fig. 10 presents the current classification for the micro-tubes with the diameters of 1.042 and 1.931 mm, where the region boundaries are drawn approximately

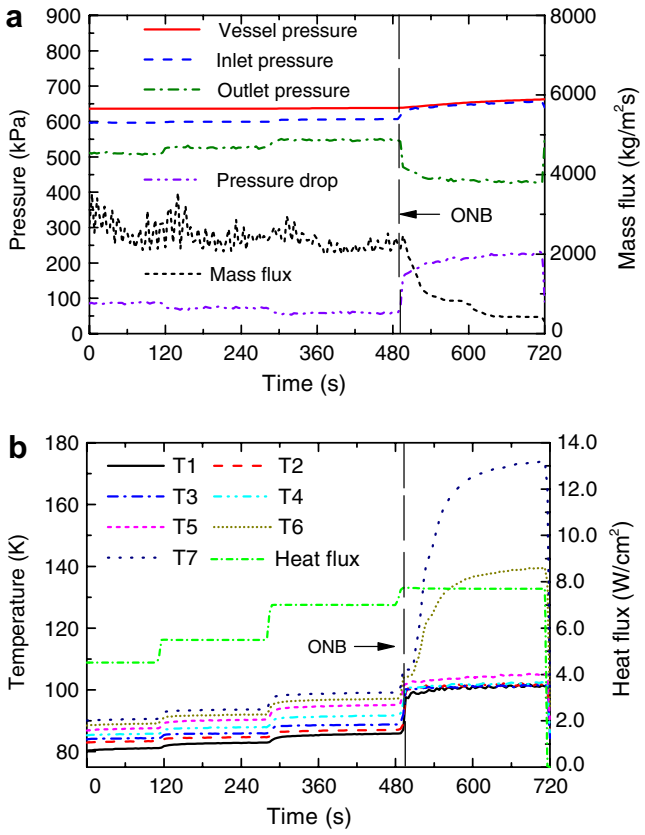

Fig. 9. The block due to the ONB for 1.042 mm micro-tube: (a) the variation of pressure and mass flux; (b) the variation of wall temperature and heat flux.

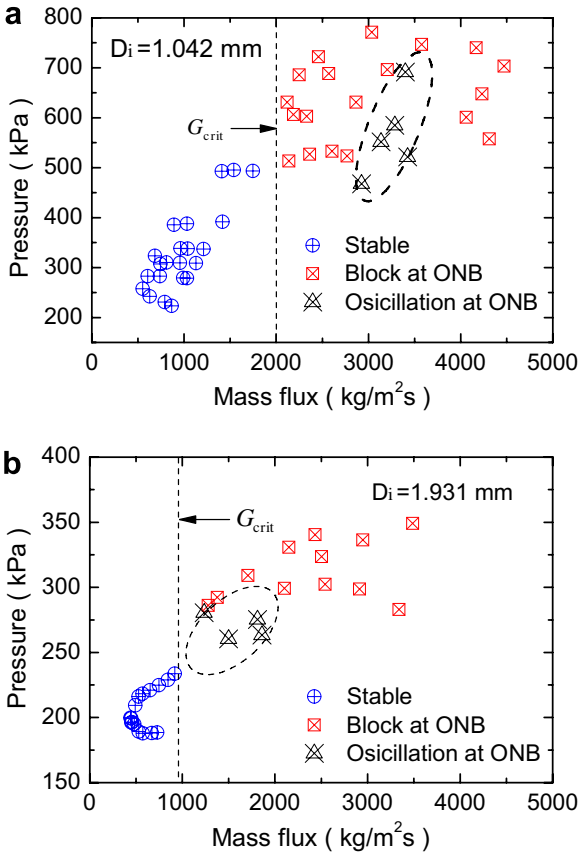

Fig. 10. Classification of stable and unstable regions: (a) 1.042 mm micro-tube; (b) 1.931 mm micro-tube.

Table 5
The parameters for the ONB block and CHF for 1.042 mm micro-tube

Class	No.	Parameters					
		T_{in} (K)	p_{in} (kPa)	G (kg/m^2 s)	q (W/cm^2)	L_{sc} (m)	x_{out}
ONB block	1	79.3	606.439	2186.1	7.70	0.248	0
	2	80.4	602.861	2330.8	7.71	0.246	0
CHF	1	78.8	283.359	590.9	11.19	0.024	0.858
	2	80.5	387.882	980.4	14.07	0.033	0.692

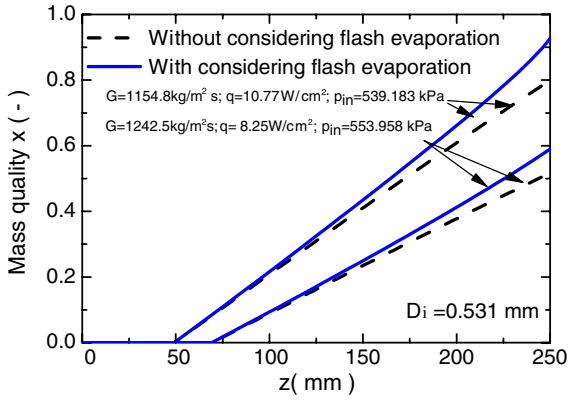

Fig. 11. The effect of flash evaporation on the mass quality.

according to the experimental data. From Fig. 10(a), it can be seen that all the experiments are divided into three regions: stable region, ONB block region and ONB oscillation region. The unstable regions including the ONB block region and ONB oscillation regions are located at high mass flux. According to mechanism analysis in the Sections 4.2.1 and 4.2.2, if the mass flux is so small that the vapor generated in the micro-tube can be discharged freely, and no vapor patch forms at the entrance of the outlet valve, the flow boiling in the micro-tube will be stable. If the generated vapor rate is close to the discharge rate from the outlet valve, a feedback between mass flux and pressure drop is built up, and a stable ONB oscillation occurs. If the generated vapor rate is larger than the discharge rate of the vapor patch, the ONB block will be observed. Hence, mass flow rate is selected as a criteria parameter. Based on Fig. 10(a) and (b), the $\dot{m}_{crit}$ can be obtained, and it is 1.71–2.64 g/s.

For the micro-tubes with the diameters of 0.531 and 0.834 mm, no ONB oscillations and ONB block are observed in the experimental range listed in Table 1. This is because their maximum mass flow rates (0.66 g/s for 0.531 mm micro-tube, 1.44 g/s for 0.834 mm micro-tube)

Table 6
Pressure drop models and correlations

Model	Equation	Remarks
Homogeneous model	$\varepsilon = \dfrac{\rho_L/\rho_G}{1/x + (\rho_L/\rho_G - 1)}$,	Both phases are assumed to flow with the same average velocity. It usually underpredicts the actual pressure drop
	$\dfrac{dp_f}{dz} = \dfrac{f_{Tp}}{D}\dfrac{G^2}{2\rho_{Tp}}$	
	where f_{Tp} is determined by Eq. (7), and	
	$\rho_{Tp} = \dfrac{\rho_G\rho_L}{\rho_G(1-x) + \rho_L x}$.	
	In Eq. (7), $Re = GD/\mu_{Tp}$, $\mu_{Tp} = x\mu_G + (1-x)\mu_L$	
L–M model	$\left(\dfrac{dp_f}{dz}\right)_{Tp} = \phi_L^2\left(\dfrac{dp_f}{dz}\right)_L$,	The effects of pressure and mass flux are not considered directly
	$\varepsilon = 1 - X(\phi_G^2)^{1/2}, \phi_L^2 = 1 + \dfrac{C}{X} + \dfrac{1}{X^2},\ \phi_G^2 = 1 + CX + X^2$	
	$\left(\dfrac{dp_f}{dz}\right)_L = \dfrac{2f_L G^2(1-x)^2}{D\rho_L},\ \left(\dfrac{dp_f}{dz}\right)_G = \dfrac{2f_G G^2 x^2}{D\rho_G}, X^2 = \dfrac{(dp_f/dz)_L}{(dp_f/dz)_G}$.	
	f_L and f_G are calculated by Eq. (7), and	
	$Re_G = \dfrac{GxD}{\mu_G}$,	
	$Re_L = \dfrac{G(1-x)D}{\mu_L}$,	
	C is the constant decided by vapor-liquid flow Reynolds number	
Chisholm B coefficient model	$\left(\dfrac{dp_f}{dz}\right)_{Tp} = \phi_{LO}^2\left(\dfrac{dp_f}{dz}\right)_{LO}$,	The effects of mass flux and fluid properties are taken into account
	$\left(\dfrac{dp_f}{dz}\right)_{LO} = \dfrac{2f_{LO}G^2}{D\rho_L}$,	
	f_{LO} is obtained by Eq. (7), and $Re_{LO} = GD/\mu_L$,	
	$\phi_{LO}^2 = 1 + (\Gamma^2 - 1)[Bx^{0.875}(1-x)^{0.875} + x^{1.75}]$,	
	$\Gamma^2 = \left(\dfrac{\mu_G}{\mu_L}\right)^{0.2}\left(\dfrac{\rho_L}{\rho_G}\right)$. B is determined by Γ :	
	$B = 55/G^{0.5}$, $0 < \Gamma < 9.5$; $B = 520/\Gamma G^{0.5}$, $9.5 < \Gamma < 28$; $B = 15000/\Gamma^2 G^{0.5}$, $28 < \Gamma$	
Friedel	$\left(\dfrac{dp_f}{dz}\right)_{Tp} = \phi_{LO}^2\left(\dfrac{dp_f}{dz}\right)_{LO}$,	
	$\phi_{LO}^2 = E + \dfrac{3.24F\cdot H}{Fr^{0.045}We^{0.035}}, E = (1-x)^2 + \dfrac{x^2\rho_L f_{GO}}{\rho_G f_{LO}}$,	
	$F = x^{0.78}(1-x)^{0.22}, H = \left(\dfrac{\rho_L}{\rho_G}\right)^{0.91}\left(\dfrac{\mu_G}{\mu_L}\right)^{0.19}\left(1 - \dfrac{\mu_G}{\mu_L}\right)^{0.7}$,	
	$Fr = G^2/gD\rho_{Tp}^2, We = G^2D/(\rho_{Tp}\sigma)$,	
	$\rho_{Tp} = \dfrac{\rho_G\rho_L}{\rho_G(1-x) + \rho_L x}$	

are less than $\dot{m}_{crit}$. The physical model also can explain why some investigation observed the ONB oscillations [10–12], but the others did not. If the mass flow rate is larger than the $\dot{m}_{crit}$ determined by the outlet constraints, the ONB oscillations occur. Otherwise, they do not. Hence, to ensure the stable operation, the determination of appropriate outlet constraints is very important in the practical design of microchannel evaporators. This is because the outlet

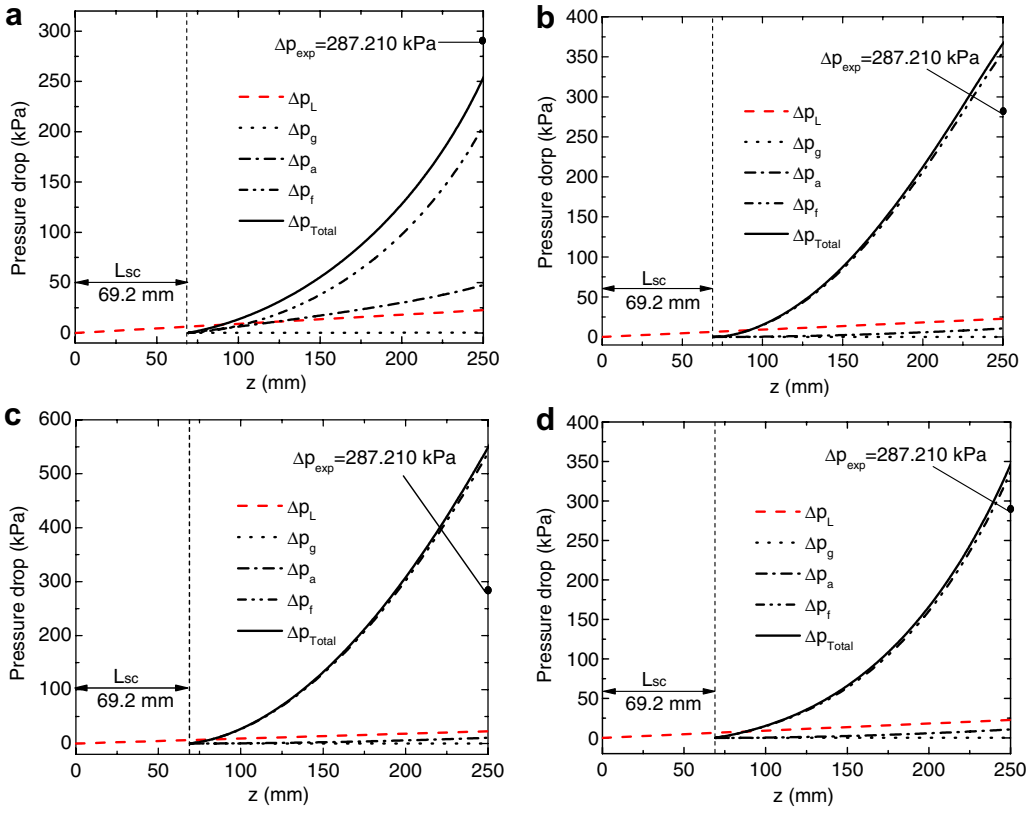

Fig. 12. The variation of three pressure drop components for different prediction model at $G = 1242.5$ kg/m^2 s, $q = 8.25$ W/cm^2 for 0.531 mm micro-tube: (a) Homogeneous model; (b) L–M model; (c) Chisholm B coefficient model; (d) Friedel model.

constraints decide the boundary of mass flow rate between stable and unstable regions.

4.2.4. Two-phase instability in the micro-tubes

In the flow boiling of liquid nitrogen in micro-tubes with the diameters of 1.042 and 1.931 mm, the long-period (50–65 s) and large-amplitude oscillations of mass flux, pressure drop and wall temperature are reported. Actually, similar oscillations are easy to appear at low mass flux and system pressure because the outlet variation may facilely affect the upstream flow in the microchannels. For example, in parallel silicon micro-tubes, Wu and Cheng [10,11] reported three kinds of unstable boiling models, i.e., the liquid/two-phase alternating flow (LTAF), the continuous two-phase flow (CTF) and the liquid/two-phase/vapor alternating flow (LTVF). The three models induce the long-period and large-amplitude oscillation. Huh et al. [12] observed the long-period (100–200 s) and large-amplitude oscillations in a rectangular single micro-tube with a hydraulic diameter of 103.5 μm. They argued that the flow pattern transition instability caused the oscillation of wall temperature, mass flux and pressure drop. However, none of them clarified what led to the transition of different flow patterns.

Huh et al. [12] had observed the coalescence of bubbles at the outlet in the experiment, but the discharge frequency was different from the frequency of the pressure, temperature, and mass flux fluctuations. Consequently they did not regard the coalescence of bubbles as the true reason for the oscillation. But they ignored the fact that the "short-period and small-amplitude" variations in the "macro-channel" of outlet plenum could be magnified, and led to "long-period and large-amplitude" oscillations in the "micro-tube".

As a whole, the essential reason for the long-period and large-amplitude oscillations of the mass flux, pressure drop and wall temperature in the micro-tubes is consider to be the vapor patch coalesced at the outlet, as shown in Fig. 7. The physical model can also explain the occurrence of the ONB block mentioned in Section 4.2.2 and the classification of stable and unstable regions in Section 4.2.3. However, further research on the theoretical model is still required to depict the oscillations by the mathematic method.

4.3. Flash evaporation quality

As mentioned in Section 3.3, flash evaporation occurs when the liquid temperature is higher than the saturated temperature corresponding to the local pressure. Fig. 11 shows the effect of flash evaporation on the mass quality. It can be seen that large discrepancy exits between the calculated results with and without the flash evaporation being considered, for example, the outlet quality of the former is about 18% higher than the latter. Comparing to the macro-channel, the local pressure in the micro-tube drops dramatically because of the large pressure drop, which will be presented in Section 4.4. Hence, x_{flash} must be taken into

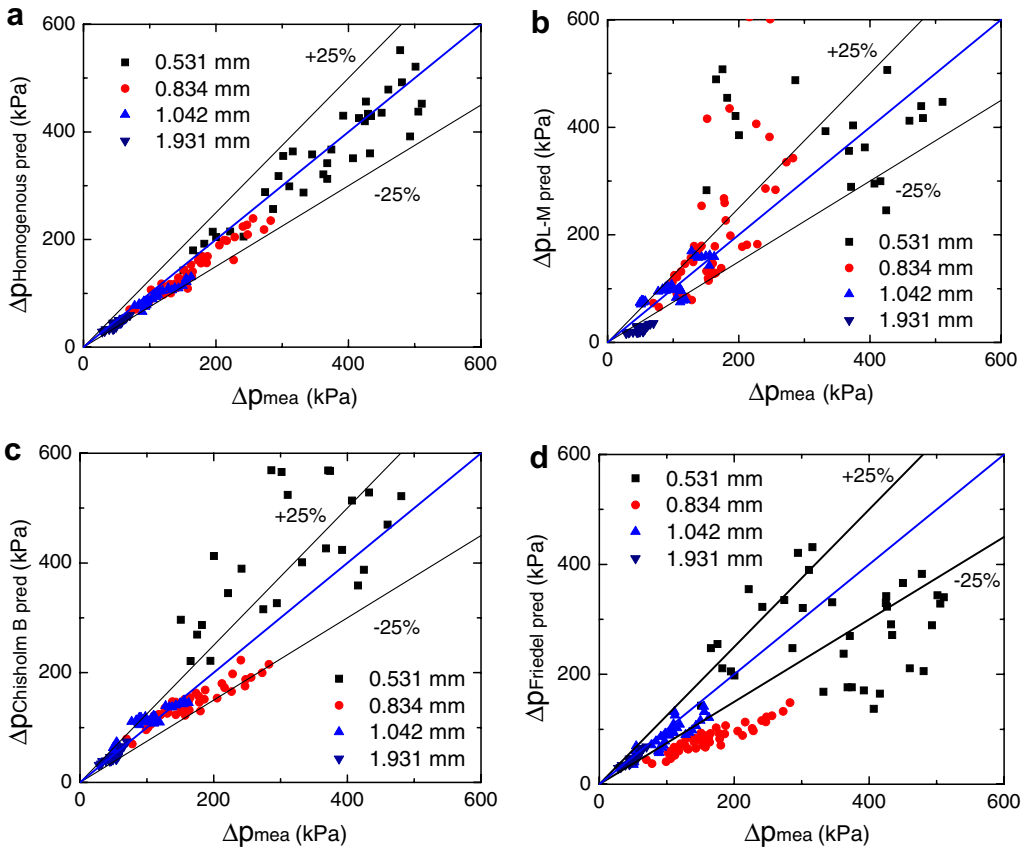

Fig. 13. Comparison of the experimental two-phase flow pressure drop to the prediction by different models: (a) Homogeneous model; (b) L–M model; (c) Chisholm B coefficient model; (d) Friedel model.

account to depict precisely the variation of mass quality along the micro-tube, instead of being ignored in the macro-channel.

4.4. Two-phase flow pressure drop

4.4.1. Analysis of the each pressure drop component

The three pressure drop components, Δp_a, Δp_g and Δp_f, can be obtained by the homogeneous model, L–M model, Chisholm B coefficient model and Friedel model, respectively. Detailed expressions for the four models [27] are listed in Table 6. Using four models, an example of two-phase pressure drop for 0.531 mm micro-tube ($G = 1242.5\ \mathrm{kg/m^2\ s}$, $q = 8.25\ \mathrm{W/cm^2}$, $\Delta p_{mea} = 287.210\ \mathrm{kPa}$) is analyzed, as shown in Fig. 12. The length of subcooled section, L_{sc}, is calculated to be 69.2 mm by the method in Section 3.2. For comparison, the pressure drop for the single-phase liquid flow pressure drop Δp_L expressed by

$$\Delta p_L = f\frac{L}{D}\frac{G^2}{2\rho_L} + \rho_L g L \tag{25}$$

and the measured pressure drop for two-phase flow Δp_{exp} are also given in Fig. 12. It can be seen that the accuracy of the homogeneous model is the best, though the prediction is slightly smaller than the measurement. Other models overestimate the experimental data obviously, and the prediction by Chisholm B coefficient model even doubles the data. The measured pressure drop in two-phase flow is dramatically higher that pure liquid flow, and $\Delta p_{mea}/\Delta p_L$ is 12.7. The frictional component is the main part of the total pressure drop, and the proportion is 81.4%, 97.1%, 98.1% and 97.2% for the homogeneous model, L–M model, Chisholm B coefficient model and Friedel model, respectively.

4.4.2. The total two-phase flow pressure drop

Totally, 135 pressure drop data for the four micro-tubes are compared respectively to the four models, as shown in Fig. 13. Contrary to the conventional channel, the homogeneous model provides the most accurate predictions for the micro-tubes, enabling to estimate all the data within an error of about ±25%. It can be explained from two aspects: (1) the flow velocity in micro-tubes is rather large, for example, it is in the range of 0.89–3.83 m/s for 0.531 mm micro-tube. And the viscosity of liquid nitrogen is very small, which will lead to high Reynolds number and more homogeneous flow. Thus, the vapor and liquid phases may mix uniformly, and form the "mist" flow, which accords with the assumption of homogeneous model that both phases flow with the same average velocity. (2) Comparing to water and refrigerants, the density ratio of liquid and vapor phases for nitrogen is smaller, which is also in favor

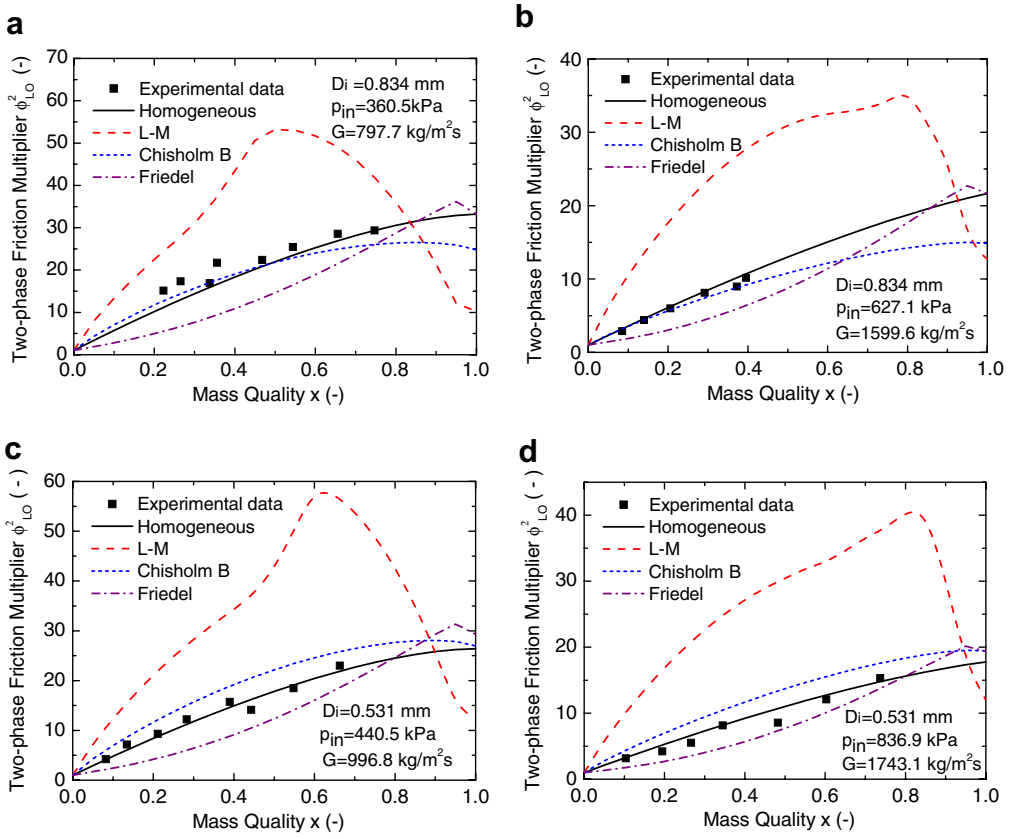

Fig. 14. The two-phase frictional pressure drop multipliers for the micro-tubes: (a) 0.834 mm micro-tube at low pressure and mass flux; (b) 0.834 mm micro-tube at high pressure and mass flux; (c) 0.531 mm micro-tube at low pressure and mass flux; (d) 0.531 mm micro-tube at high pressure and mass flux.

of the prediction by homogeneous model. Even for the two-phase flow in the tube with a diameter of 14.0 mm, the homogeneous model can predict the data well [28]. Ribatski et al. [29] and Vassallo and Keller [30] also proved that the homogeneous model could provide the best perdition for the conditions of high pressure and large mass flux. Except the data for 0.531 mm micro-tube, Chisholm B coefficient model can yield good prediction for the measured two-phase pressure drop. The error for L–M model and Friedel model is so large that they are not recommended for predicting two-phase flow pressure drop of liquid nitrogen in micro-tubes.

Actually, the result can also be explained from the two-phase flow pattern. Though there is no flow pattern investigation on the flow boiling of liquid nitrogen in micro-tube at present, the observations for other fluids in micro-tube can shed the light on this point. Based on the careful visualization, Lee and Mudawar [16] pointed out that the flow patterns for the refrigerants may different from those for water because the low surface tension of R-134a can produce far smaller bubbles than in water. Very small bubbles are much apt to travel discretely along a microchannel before coalescing into long bubbles, thus enabling the bubbly and slug flow regimes to be more prevalent in refrigerant micro-tube flow. Pettersen [31] observed the flow was annular and with a "mist" flow of liquid droplets in the core for CO_2 at mass flux of 580 kg/m^2 s. It is well known that the surface tension of liquid nitrogen is smaller than that of R-134a. Hence, the dominant flow pattern of liquid nitrogen in micro-tube is considered to be the discrete bubble flow at low and medium mass quality, and the annular flow with a "mist" core of liquid droplets. The dominant flow pattern makes it possible that the pressure drop can be predicted well by the homogeneous model.

4.4.3. Two-phase frictional pressure drop multipliers

In the analysis of Sections 4.4.1 and 4.4.2, the total pressure drop is the integral along the micro-tube length because the mass quality varies along the flow direction. To investigate the relationship between mass quality and the friction pressure drop, the two-phase frictional pressure drop multipliers for the micro-tubes are measured for different mass quality according to method expressed in Section 2.2. Figs. 14(a) and (b) present the results for 0.834 mm micro-tube at different pressure and mass flux. It can be seen that the homogeneous model gives the best agreement with the experimental data, as explained in Section 4.4.2. Comparison of Figs. 14(a) and (b) demonstrates that the effect of pressure and mass flux on the homogeneous model's performance is very small because it works well in both cases. Chisholm B coefficient model

can well predict the data for 0.834 mm micro-tube. L–M model overestimates the data obviously; sometimes, the prediction even three times the measurement. However, Friedel model underestimates the present data significantly. Other measured results for the micro-tubes with the diameters 1.042 and 1.931 mm also show the same trends. For 0.531 mm micro-tube, the two-phase multiplier can also be described by the homogeneous model as shown in Figs. 14(c) and (d). The validity of Chisholm B coefficient model decreases as the tube diameter becomes smaller, and the over-prediction is observed for 0.531 mm micro-tube.

5. Conclusions

The flow boiling characteristics of liquid nitrogen in micro-tubes with the diameters of 0.531, 0.834, 1.041 and 1.931 mm are investigated systematically. This part focuses on the ONB, two-phase flow instability and two-phase flow pressure drop. Main conclusions are drawn as follows:

(1) ONB can be marked by the phenomena that mass flux drops suddenly while pressure drop increases, and apparent wall temperature hysteresis in the range of 1.0–5.0 K occurs. The fitting based on the Thom model enables to predict the wall superheat and heat flux well at ONB.
(2) Stable oscillations of pressure drop, mass flux and wall temperatures are observed at ONB for the micro-tubes with the diameters of 1.042 and 1.931 mm. These oscillations are characterized by long-period (50–60 s) and large-amplitude. The phase difference between the pressure drop and mass flux oscillations is about 180°. The wall temperature oscillations own the same phase to the pressure drop. Block phenomenon is also observed at ONB in case of high pressure and mass flux. The regions for the oscillations, block and stable flow boiling are classified.
(3) A physical model is proposed to explain the ONB oscillations and block phenomenon. The essential reason is considered being the vapor patch coalesced at the outlet, which causes the flow pattern alternative transition between liquid phase and vapor phase in micro-tubes. Mass flow rate is selected as a criterion parameter to classify three regions: oscillations region, block region and the stable flow boiling region. If the mass flux is so small that the vapor generated in the micro-tube can be discharged freely, and no vapor patch forms at the entrance of the outlet valve, the flow boiling in the micro-tube will be stable. If the generated vapor rate is close to the discharge rate from the outlet valve, a feedback between mass flux and pressure drop is built up, and a stable ONB oscillation occurs. If the generated vapor rate is larger than the discharge rate of the vapor patch, the ONB block will be observed.
(4) Contrary to the conventional channel, homogeneous model enables to predict the experimental data of two-phase flow pressure drop well, and the prediction divergences of three separated flow models are rather large. It can be explained by the fact that the density ratio of liquid to vapor for nitrogen is comparatively small, and the liquid and vapor phases may mix well in micro-tube at high mass flux due to small viscosity of liquid nitrogen, which leads to a more homogeneous flow.

Acknowledgments

This research is jointly supported by A Foundation for the Author of National Excellent Doctoral Dissertation of PR China (200236), National Natural Science Foundation of China (50776057 and 50436030) and NCET.

References

[1] Y.Y. Hus, On the size range of active nucleation cavities on a heating surface, J. Heat Transfer 84 (1962) 207–216.
[2] T. Sato, H. Matasumura, On the conditions of incipient subcooled-boiling with forced convection, Bull. JSME 7 (1963) 392–398.
[3] A.E. Bergles, W.M. Rohsenow, The determination of forced-convection surface-boiling heat transfer, J. Heat Transfer 86 (1964) 365–372.
[4] I. Hapke, H. Boye, J. Schmidt, Onset of nucleate boiling in minichannels, Int. J. Therm. Sci. 39 (2000) 505–513.
[5] S.M. Ghiaasiaan, R.C. Chedester, Boiling incipience in microchannels, Int. J. Heat Mass Transfer 45 (2002) 4599–4606.
[6] D. Liu, P.S. Lee, S.V. Garimella, Prediction of the onset of nucleate boiling in microchannel flow, Int. J. Heat Mass Transfer 48 (2005) 5134–5149.
[7] S. Kakac, L. Cao, M.R. Avelino, The effect of inlet subcooling on two-phase flow dynamic instabilities in-tube boiling systems, Low Temperature and Cryogenic Refrigeration, Kluwer Academic Publisher, 2003.
[8] L. Zhang, J. Koo, L. Jiang, K.E. Goodson, J.G. Santigo, T.W. Kenny, Study of boiling regimes and transient signal measurements in microchannel, in: Proc. Transducers'01, Munich, Germany, 2001, pp. 1514–1517.
[9] G. Hetsroni, A. Mosyak, E. Pogrebnyak, Z. Segal, Explosive boiling of water in parallel microchannel, Int. J. Heat Mass Transfer 31 (2005) 371–392.
[10] H.Y. Wu, P. Cheng, Visualization and measurements of periodic boiling in silicon microchannels, Int. J. Heat Mass Transfer 46 (2003) 2603–2614.
[11] H.Y. Wu, P. Cheng, Boiling instability in parallel silicon microchannels at different heat flux, Int. J. Heat Mass Transfer 47 (2004) 3631–3641.
[12] C. Huh, J. Kim, M.H. Kim, Flow pattern transition instability during flow boiling in a single microchannel, Int. J. Heat Mass Transfer doi:10.1016/j.ijheatmasstransfer.2006.07.027.
[13] P.M.Y. Chung, M. Kawaji, The effect of channel diameter on adiabatic two-phase flow characteristics in small tubes, Int. J. Multiphase Flow 30 (2004) 735–761.
[14] D.S. Wen, D.B.R. Kenning, Two-phase pressure drop of water during flow boiling in a vertical narrow channel, Exp. Therm. Fluid Sci. 28 (2004) 131–138.
[15] W. Yu, D.M. France, M.W. Wambsganss, J.R. Hull, Two-phase pressure drop, boiling heat transfer, and critical heat flux to water in a small-diameter horizontal tube, Int. J. Multiphase Flow 28 (2002) 927–941.

[16] J. Lee, I. Mudawar, Two-phase flow in high-heat-flux micro-channel heat sink for refrigeration cooling applications: Part I – Pressure drop characteristics, Int. J. Heat Mass Transfer 48 (2005) 928–940.
[17] M. Zhang, R.L. Webb, Correlation of two-phase friction for refrigerants in small-diameter tubes, Exp. Therm. Fluid. Sci. 25 (2001) 131–139.
[18] R. Revellin, J.R. Thome, Adiabatic two-phase frictional pressure drops in microchannels, Exp. Therm. Fluid Sci. doi:10.1016/j.expthermflusci.2006.07.001.
[19] V.V. Klimenko, Heat transfer intensity at forced flow boiling of cryogenic liquids in tubes, Cryogenics 22 (1982) 569–576.
[20] S.L. Qi, P. Zhang, R.Z. Wang, L.X. Xu, Single-phase pressure drop and heat transfer characteristics of turbulent liquid nitrogen flow in micro-tubes, Int. J. Heat Mass Transfer (2006), doi:10.1016/j.ijheatmasstransfer.2006.09.032.
[21] B.J. Moffat, Describing the uncertainties in experimental results, Exp. Therm. Fluid Sci. 1 (1988) 3–17.
[22] J.R.S Thom, W.M. Walker, T.A. Fallon, G.F.S. Reising, Boiling in subcooled water during flow up heated tubes or annuli, in: Symposium on Boiling Heat Transfer in Steam Generating Units and Heat Exchangers, Manchester, September 1965, ImechE, London, 1965.
[23] X.F. Peng, B.X. Wang, Forced-convection and boiling characteristics in microchannels, in: Proceedings of 11th International Heat Transfer Conference, Kyongju, Korea, vol. 1, 1998, pp. 371–390.
[24] T.H. Yen, N. Kasagi, Y. Suzuki, Forced convective boiling heat transfer in microtubes at low mass and heat fluxes, Int. J. Multiphase Flow 29 (2003) 1771–1792.
[25] J. Li, P. Cheng, Bubble cavitation in a microchannel, Int. J. Heat Mass Transfer 47 (2004) 2689–2698.
[26] Q. Wang, X.J. Chen, Y. Ding, Boiling onset oscillation: a new type of dynamic instability in a forced-convection upflow boiling system, Int. J. Heat Fluid Flow 17 (1996) 418–423.
[27] J.J. Xu, Flow boiling heat transfer and liquid-vapor two-phase flow, Nuclear Energy, second ed., Beijing, 2001, pp. 100–123.
[28] D. Steiner, E.U. Schlunder, Heat transfer and pressure drop for boiling nitrogen flowing in a horizontal tube 2. Pressure drop, Cryogenics 16 (1976) 457–464.
[29] G. Ribatski, L. Wojtan, J.R. Thome, An analysis of experimental data and prediction methods for two-phase frictional pressure drop and flow boiling heat transfer in micro-scale channels, Exp. Therm. Fluid Sci. doi: 10.1016/j.expthermflusci.2006.01.006.
[30] P. Vassallo, K. Keller, Two-phase frictional pressure drop multipliers for SUVA R-134a flowing in a rectangular duct, Int. J. Multiphase Flow 32 (2006) 466–482.
[31] J. Pettersen, Flow vaporization of CO_2 in microchannel tubes, Exp. Therm. Fluid Sci. 28 (2004) 111–121.